ADVANCED ENERGY MATERIALS
www.advenergymat.de

Two Channels of Charge Generation in Perylene Monoimide Solid-State Dye-Sensitized Solar Cells

Ian A. Howard, Michael Meister, Björn Baumeier, Henrike Wonneberger, Neil Pschirer, Rüdiger Sens, Ingmar Bruder, Chen Li, Klaus Müllen, Denis Andrienko, and Frédéric Laquai**

The mechanism of charge generation in solid-state dye-sensitized solar cells using triarylamine-substituted perylene monoimide dyes is studied by vis-NIR broadband pump-probe transient absorption spectroscopy. The experiments demonstrate that photoinduced electron injection into the TiO_2 can only occur in regions where Li^+, from the commonly used Li-TFSI additive salt, is present on the TiO_2 surface. Incomplete surface coverage by Li^+ means that some dye excitons cannot inject their electron into the TiO_2. However it is observed in the solar cell structure that some of the dye excitons that cannot directly inject an electron still contribute to free charge generation by the previously hypothesized reductive quenching mechanism (hole transfer to the solid-state hole transporter followed by electron injection from the dye anion into the TiO_2). The contribution of reductive quenching to the quantum efficiency of charge generation is significant, raising it from 68% to over 80%. Optimization of this reductive quenching pathway could be exploited to maintain high quantum efficiency in dyes with greater NIR absorption to achieve overall enhancements in device performance. It is demonstrated that broadband NIR transient spectroscopy is necessary to obtain population kinetics in these systems, as strong Stark effects distort the population kinetics in the visible region.

1. Introduction

Dye-sensitized solar cells (DSCs) are promising photovoltaic devices for solar energy conversion in the current quest for sustainable sources of electrical energy. Since their invention in 1991,[1] the power conversion efficiency of liquid-electrolyte based solar cells has increased steadily mainly due to design of dye molecules and redox partners with current record efficiencies now up to 12.3%.[2] Although the record solar cells use a less corrosive cobalt-based liquid electrolyte instead of the common iodide-iodine redox couple, the use of a liquid electrolyte to achieve hole transport limits their employment in large-scale industrial production. Many research groups currently try to replace the liquid electrolyte by a solid-state hole transporter, however, efficiencies still lag behind the liquid-electrolyte analogues for reasons not yet entirely understood. Several approaches have been pursued including inorganic,[3] polymer-based[4] and organic small molecule hole transport materials. Efficiencies as high as 7.2% have been reported for the latter,[5] employing 2,2′,7,7′-tetrakis(N,N-di-p-methoxyphenylamine)-9,9′-spirobifluorene (spiro-MeOTAD)[6] as the solid-state hole transport material. The mesoporous TiO_2 layer must be thinner in solid-state DSCs (i.e., only a few micrometers thick) than in liquid-electrolyte cells[7] and thus it is very important to use dyes with strong absorption and high surface coverage leading to maximized harvesting of the incident solar light. In this respect organic dyes are excellent candidates[5] due to their high molar extinction coefficients. In particular perylene monoimides, which have excellent photo and thermal stability and are often used as color pigments,[8] have attracted significant attention as sensitizers in dye-sensitized solar cells, as electron transporters in bulk heterojunction solar cells,[9] and also as high mobility charge transport materials in organic field-effect transistors.[10] High efficiencies in solid-state DSCs have already been achieved by using perylene imide derivatives of a donor-spacer-acceptor type structure.[11] However, there are currently only very few studies addressing the mechanism of charge generation in solid-state organic (metal-free) dye-sensitized solar cells in general and in perylene-based dye-sensitized cells in particular.[12–14] We note that recent results achieved using inorganic perovskite coatings as a sensitizer/hole-transport material have achieved very impressive power conversion efficiencies exceeding 10%.[3,15,16]

Dr. I. A. Howard, Dr. M. Meister, Dr. F. Laquai
Max Planck Research Group for Organic Optoelectronics
Synthetic Chemistry Group, Polymer Theory Group
Max Planck Institute for Polymer Research
Ackermannweg 10, 55128, Mainz, Germany
E-mail: ian.howard@mpip-mainz.mpg.de;
laquai@mpip-mainz.mpg.de
Dr. B. Baumeier, Dr. D. Andrienko
Polymer Theory Group
Max Planck Institute for Polymer Research
Ackermannweg 10, 55128, Mainz, Germany
Dr. H. Wonneberger, Dr. N. Pschirer, Dr. R. Sens, Dr. I. Bruder
BASF SE, GVE/E – J542, 67056
Ludwigshafen, Germany
Dr. C. Li, Prof. K. Müllen
Synthetic Chemistry Group
Polymer Theory Group
Max Planck Institute for Polymer Research
Ackermannweg 10, 55128, Mainz, Germany.

DOI: 10.1002/aenm.201300640

(I) $S + D^{*} + TiO_2 \rightarrow S^{+} + D^{+} + TiO_2^{-} \rightarrow S^{++} + D + TiO_2^{-}$

(II) $S + D^{*} + TiO_2 \rightarrow S^{++} + D^{-} + TiO_2 \rightarrow S^{++} + D + TiO_2^{-}$

Figure 1. Two possible types of charge generation in solid-state dye-sensitized solar cells. S is the spiro hole transport material, D is the dye, TiO_2 is the titania, +/– indicates cation/anion and * indicates exciton. In type I, the electron is injected from the excited dye to the TiO_2, which is then regenerated by the hole transporter (I). In type II charge generation, the electron is first transferred from the hole transporter to the excited dye and subsequently injected into the TiO_2 (II).

The cascade of processes leading to charge generation after absorption of a photon by the dye is often described as 1) electron injection from the excited state of the dye into the TiO_2 conduction band followed by 2) regeneration of the dye cation remaining after electron injection by the hole transport material or liquid electrolyte,[17] which hereafter we address as type I charge generation (see **Figure 1**). In fact, in liquid electrolyte cells this type I pathway for charge generation is the only one possible, because the regeneration of the dye cation is diffusion-limited and hence occurs typically on a timescale of nano- to microseconds, i.e., much slower than electron injection, which can lead to a photocurrent loss, if the recombination of electron and dye cation is on a similar timescale.[17] In solid-state dye-sensitized cells type I charge generation is not necessarily the only mechanism for charge separation. In fact, a second mechanism named reductive quenching has already been proposed.[13] In solid-state cells, the hole transporter is in close proximity to the dye and thus electron transfer from the hole transporter to the photoexcited state of the dye (equivalently described as hole injection from the photoexcited dye into the hole transport material) could take place on the timescale of a few picoseconds.[12] In this case, a second pathway of free charge generation is opened, which is reduction of the excited state of the dye by the hole-transporter followed by electron injection from what is now a dye anion into the titania nanoparticles. We note that the injection of the electron from the dye anion can be significantly more energetically favorable than injection of the electron from the dye exciton. Hereafter, we call this mechanism type II charge generation (see Figure 1). If type I charge generation is impeded, type II charge generation could take over and help deliver a higher overall quantum efficiency for charge generation. The possible importance of type II generation has been highlighted by Snaith et al.[13] and it has been shown that perylene imide dyes mixed into a spiro-MeOTAD matrix are quenched after photo excitation by hole transfer from the dye exciton to the spiro-MeOTAD matrix.[14] However, to the best of our knowledge, direct experimental evidence demonstrating that type II charge generation occurs in solid-state dye-sensitized solar cells has not been presented yet. This direct evidence for type II charge generation is presented herein, where we show that it plays an important role in determining the quantum efficiency of charge generation in this dye system where electron injection from the dye exciton into the TiO_2 is borderline. In fact, our key finding is that for the dye used in this study the electron injection from a dye exciton requires the presence of nearby surface-localized Li^+ cations from the often used additive Bis(trifluoromethane)sulfonimide lithium salt (Li-TFSI). When these cations are not in the direct vicinity of a dye exciton it cannot participate in type I charge generation, but it can still participate in type II charge generation meaning that a significant fraction of the non-Li^+-affected excitons also eventually lead to free charges allowing the cell a good overall quantum efficiency.

2. Results and Discussion

2.1. Device Performance

Figure 2 shows the chemical structures of the perylene imide derivative used as sensitizer and the solid-state hole transport material spiro-MeOTAD along with typical current–voltage (*J–V*) characteristics of devices. We could achieve power conversion efficiencies as high as 4% with this particular material system. The maximum photon to electron conversion efficiency (internal quantum efficiency, IQE) of this dye was found to be

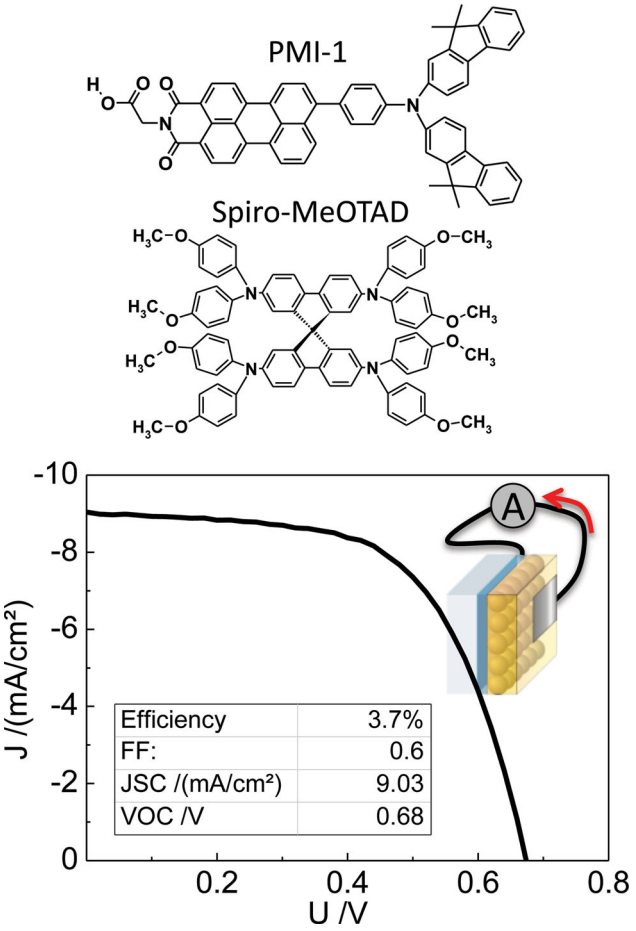

Figure 2. Chemical structures of the perylene monoimide sensitizer PMI-1 (top) and of the hole transport material spiro-MeOTAD (middle). Typical *J–V*-characteristics of a dye-sensitized solar cell are depicted in the bottom graph. The inset shows a schematic of a solid-state DSC comprised of a glass substrate, a transparent conductive layer (FTO), a dyed mesoporous TiO_2 layer incorporated with the solid hole transporter and a silver counter electrode.

Adv. Energy Mater. **2013**,
DOI: 10.1002/aenm.201300640

about 67%. In this system, as in many others, the additive Li-TFSI plays an important role for the device efficiency, since it influences not only the charge transport properties of the hole transport material,[18] but also, as we will see in the following section, the injection efficiency of electron transfer from the dye into the TiO_2.

2.2. Optical Spectroscopy

2.2.1. Samples

In order to understand the role of type I and type II charge generation we used steady-state, quasi-steady-state, and time-resolved optical spectroscopy to investigate a sequence of three samples consisting of: 1) dye attached to titania, 2) dye attached to titania in presence of Li-TFSI, and 3) a full solar cell structure with the hole transporting material and Li-TFSI but omitting the metal electrode. Full sample preparation details are provided in the Supporting Information along with experimental details.

2.2.2. Quasi-Steady-State Photoinduced Absorption

Quasi-steady-state photoinduced absorption (PIA) records the change of absorption of a sample due to long-lived photoinduced excited states, such as charges created in dye-sensitized solar cells.[19] **Figure 3** depicts the steady-state PIA spectra of the three samples. In sample 1, the surface bound dye without the Li-TFSI additive, no photoinduced signal was observed

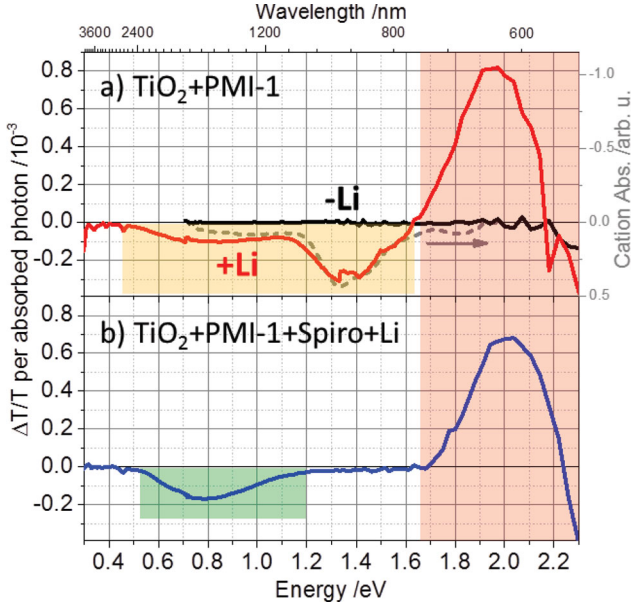

Figure 3. Quasi-steady-state photoinduced absorption spectra of a) sample 1 (black line) and sample 2 (red line) along with the absorption spectrum of the chemically oxidized dye (dye cation) shown as a dashed gray line. b) The PIA spectrum of the device-like structure including the hole transporter spiro-MeOTAD and the additive Li-TFSI. Highlighted in red is the bleaching/Stark effect region, in yellow the dye cation absorption and in green the absorption of the spiro cation.

indicating that no long-lived charges are created in this sample. In contrast, sample 2 which is identical to sample 1 except that the Li-TFSI is added, showed a strong induced absorption due to long-lived charges. The charge-induced absorption spectrum shows a positive signal in the higher energy region of the spectrum with a zero crossing at 760 nm (1.63 eV), which can be assigned to the ground state bleaching of those dye molecules that had successfully injected electrons into the TiO_2 plus a Stark effect due to the influence of the fields of the photoinduced charges on the ground state absorption of the nearby dye molecules. A strong photoinduced absorption was observed in the near IR region peaking around 900 nm (1.38 eV), which extended further into the IR. This feature is very similar to that of the chemically oxidized dye (shown for comparison as the dashed gray line) supporting our assignment of this photoinduced spectrum to the creation of dye cations.

From the comparison of sample 1 and sample 2 by PIA we reach our first key conclusion: in this dye system, Li-TFSI must be present for electron injection from a dye exciton into the titania to occur.

In sample 3, when the hole transport material spiro-MeOTAD is also present, the induced absorption of the long-lived charges changes from that in sample 2. This is because the dye cation is reduced by hole transfer to the hole transport material in sample 3, so the long-lived states are the oxidized hole transport material and an electron in titania rather than the dye cation and electron in titania present in sample 2. Looking at the spectrum of sample 3 it is clear that the dye cation photoinduced absorption feature at 900 nm vanishes entirely, while a different photoinduced absorption feature peaking in the NIR region around 1550 nm (0.8 eV) emerges. This new absorption band can be assigned to the cation of the hole transport material spiro-MeOTAD by comparison with previously published results.[20–22] As the PIA of the dye cations was found to be entirely absent in the presence of spiro-MeOTAD, it appears that the pore filling was sufficient to regenerate virtually all oxidized dye molecules. Since the regeneration of the dye cations restores the ground state of the dye molecules, a ground state bleaching caused by dyes in an excited state no longer exists, however the Stark effect on ground state dyes of the photoinduced field leads to a very strong positive signal in the short wavelength region (1.7 to 2.2 eV).[23]

This Stark effect has recently been examined in detail by us and others, in order to provide insight into the motion of charges near the interface.[23–25] In order to investigate the role of type I and type II mechanisms in the generation of the free charges in sample 3 we must turn to time-resolved spectroscopy, however the PIA of sample 3 reveals a second key conclusion, namely that pore-filling is good enough to allow complete dye regeneration, as no feature of the dye cation remains in the photoinduced absorption of sample 3.

2.2.3. Steady-State Spectroscopy

The steady-state absorption spectra of samples 1, 2, and 3 are presented in **Figure 4**a. The addition of Li-TFSI in sample 2 causes a change in the ground state absorption spectrum relative to that in sample 1. The absorption is broadened and red-shifted. Similarly in sample 3 a clear broadening and a red

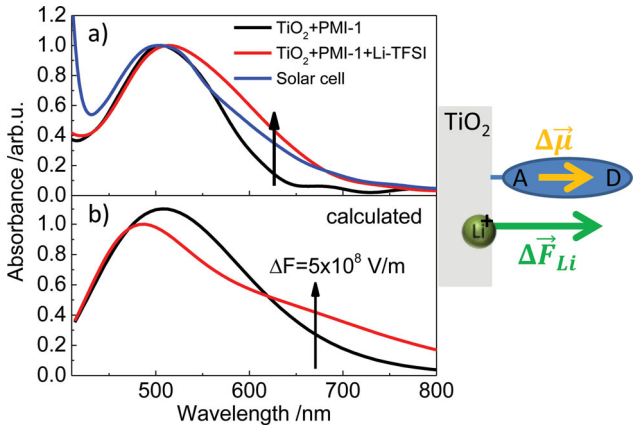

Figure 4. a) Absorption spectra of PMI-1 dyes attached to TiO_2 in the absence and presence of Li^+-ions. Note the emergence of a shoulder in the absorption spectrum upon addition of Li-TFSI. b) Field-dependent absorption spectra of PMI-1 calculated by TDDFT. A positive change in electric field ($\Delta\vec{F}$) corresponds to a field change pointing away from the TiO_2 surface. Note that for a less negative field, i.e. a more positively charged TiO_2, a shoulder at the red edge of the spectrum occurs. c) Comparison of the normalized absorption spectra of PMI-1 on titania in the absence of Li-TFSI, in the presence of Li-TFSI and in the device-like structure including spiro-MeOTAD and Li-TFSI. The sketch on the right side depicts schematically the positive change in electric field $\Delta\vec{F}$ due to the Li^+-ions and the direction of the change in dipole moment from the ground to the excited state $\Delta\vec{\mu}$.

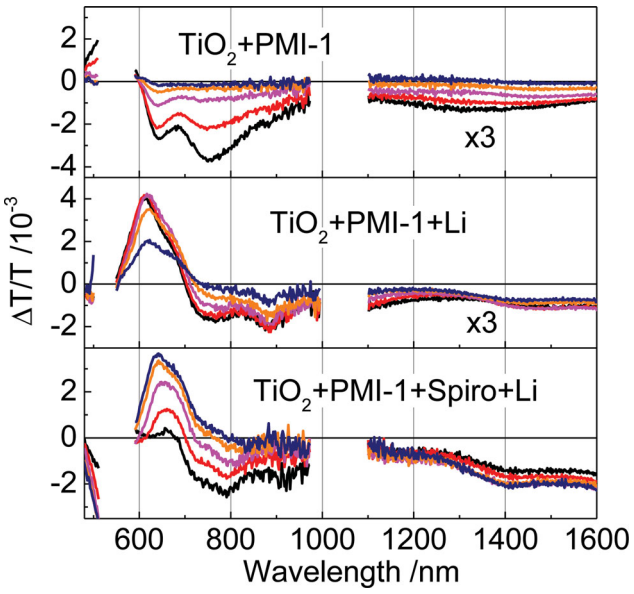

Figure 5. Transient absorption spectra (averaged over time) of PMI-1 adsorbed on TiO_2 (sample 1, upper panel), with Li-TFSI (sample 2, middle panel) and in the device-like structure with Li-TFSI and spiro-MeOTAD (sample 3, bottom panel). Colors refer to mean delay times as follows: black: 1.25 ps; red: 3.8 ps; magenta: 34 ps; orange: 335 ps; violet: 3125 ps.

shoulder are observed. The effect of Li-TFSI on the absorption spectra can be explained by the Stark effect of Li^+ ions adsorbed to the titania surface.

Considering the Stark effect, i.e. the influence of an electric field on the ground state absorption, we note the following:[23] a zeroth order approximation would be that an electric field antiparallel to the change of the electric dipole moment $\Delta\mu$ of the dye shifts the absorption peaks to higher energies, whereas a field parallel to the change of the dipole moment causes shifts to lower energies. This would suggest that there is a parallel field present, at least in sample 2, and as shown in Figure 4 the field created by a surface adsorbed Li^+ ion is indeed parallel. The precise effect of field on absorption, taking into account both peak shifts and changes in oscillator strength (which are both found to be important) can be calculated by time-dependent density functional theory (TDDFT). Figure 4b shows the absorption spectrum as calculated for PMI-1 in the gas phase with and without a parallel applied electric field. Qualitatively the calculated Stark effect matches very well with the observed absorption changes, leading us to our third key conclusion: that the broad red shoulder observed in the absorption spectrum of sample 2 and 3 indicate that surface adsorbed Li^+ ions are present in both of these samples, and that these surface bound Li^+ ions create fields that lower the barrier for charge injection.

2.2.4. Transient Absorption Spectra

Figure 5 compares the time-resolved absorption spectra of three samples in the time range from 1 ps to 3 ns. The transient pump-probe spectra of the first sample (dye on titania, upper panel) exhibit a positive signal in the short wavelength spectral region, which we assign to ground state bleaching. It then has a zero crossing at 600 nm followed by a broad photoinduced absorption at longer wavelength extending into the near-infrared spectral region. All features decayed within the observed time range of 3 ns without drastic change in spectral shape indicating that long-lived charges were not created in this sample in good agreement with the PIA results presented above. We stress that neither a negative PIA peak around 900 nm nor a Stark contribution in the visible is observed, meaning that no dye cations are created, so the transient signal recorded measures the return of dye excitons to the ground state under the influence of the titania surface environment. Consistent with our interpretation of the PIA, no charges are created in sample 1 (which contains no Li-TFSI).

In sample 2 (middle panel) the measured signal is substantially different. Firstly there is clear evidence that charges are created. The spectrum by 3 ns resembles strongly that of charges observed in the quasi-steady-state PIA spectroscopy. For a direct comparison of the PIA spectrum and 3 ns time-resolved spectrum of sample 2 (see Supporting Information). Also in the supporting information we measure the decay of this cation signal on the ns to ms timescale and find that its decay is consistent with carrier recombination kinetics. From this information it is clear that the excited states remaining in sample 2 after 3 ns are exclusively dye cations and electrons in titania, but the spectral evolution before 3 ns indicates that other species are present at earlier times. The pronounced peak at 770 nm at early times can be seen to be a feature of exciton induced absorption from comparison with sample 1. In sample 2 this peak is present in the short-delay spectra but disappears gradually from the longer-delay spectra. This

Adv. Energy Mater. **2013**,
DOI: 10.1002/aenm.201300640

indicates that some fraction of the population created after the instrument response of our spectrometer is in the exciton population pool and that this population fraction decays similarly to how it decays in sample 1. So a fourth key conclusion is that not all dye excitons can promptly inject an electron into the titania in sample 2. In the further analysis we will find that these data from sample 2 are best described by two populations being present after the instrument response, one population of dye cations that are relatively long-lived (these are created by excitons which inject their electron into the titania within the instrument response of the system), and one population of excitons that then decay exactly as they did in sample 1 indicating that they are completely uninfluenced by Li-TFSI most likely because there is not any in their vicinity.

The TA spectra of sample 3 at early times in the visible wavelength region are quite similar to those of sample 2. Both spectra show Stark effect-induced features which dominate the visible wavelength region up to 750 nm. However there are also two important differences. Firstly, the negative feature observed at 900 nm in the spectra for sample 2 which can be ascribed to the dye cation are absent in the spectra of sample 3 after 2 ps. Also, the PIA of the oxidized spiro at 1550 nm quickly grows in then remains almost constant. This again confirms our quasi-steady-state PIA conclusion that pore-filling is sufficient for dye reduction, we see no fraction of dye cations that are not quickly reduced by hole transfer to nearby hole transport material. Also in sample 3, the features of the exciton population, most clearly visible at the 770 nm photoinduced absorption peak no longer decay as they do in sample 1, but rather they disappear much more quickly. This indicates that the exciton population in sample 3 is quenched by a process not present in sample 1 or 2. Thus, in sample 3 the dye excitons that could not inject charges into the titania in sample 2 exhibit a shortened lifetime in sample 3 indicating that they can create charges by the now available type II mechanism.

2.2.5. Introduction to Modeling of Transient Kinetics

In the preceding sections we have, amongst others, made the key conclusions that: 1) in sample 2 only some fraction, let us say *f*, of dye excitons can promptly inject an electron into the titania. The remaining $(1 - f)$ excitons decay as they did in sample 1 and 2) in sample 3 the remaining $(1 - f)$ excitons no longer decayed as they did in sample 1, but rather where quenched through type II charge generation.

In the coming section we will consider the transient absorption data of sample 1 and sample 2 to estimate *f*, the fraction of dye excitons that participate in type I charge generation. We will then use a simple photophysical model to fit the transient absorption data of sample 3 from which we can extract how much the overall quantum efficiency of the device is increased by type II charge generation in the $(1 - f)$ dye excitons which cannot participate in type I charge generation.

2.2.6. Transient Kinetics: Sample 1 and 2 (determination of f)

The transient absorption kinetics of sample 1 are depicted in **Figure 6**a. We show three wavelength regions chosen to be useful for the comparison of samples 1, 2 and 3. Although in sample 1 excitons are the only species present, the wavelength regions chosen are selected so that when a mixture of excited state species is present good contrast between the species is achieved. In the 800–810 nm region dye excitons have the dominant cross-section, between 850–950 nm the dye cations have the dominant cross-section, and between 1400–1600 nm the spiro cations have the dominant cross-section.

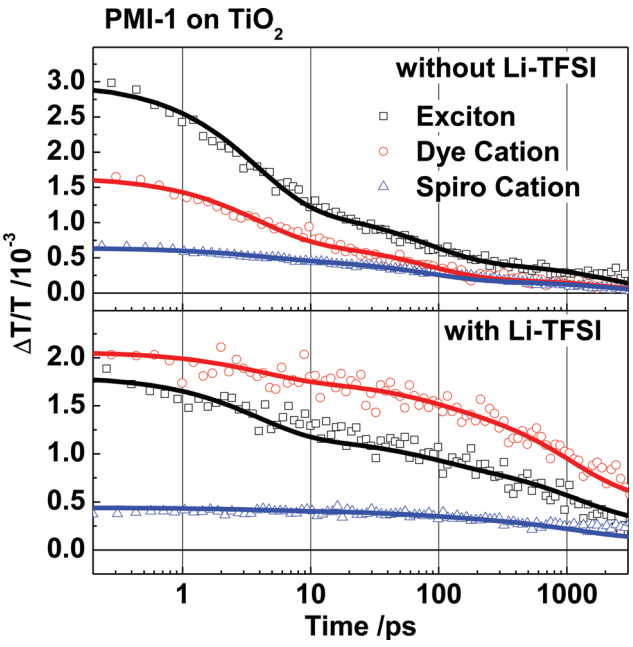

Figure 6. Transient absorption kinetics monitored at 805 nm (black squares), 900 nm (red circles) and 1500 nm (blue triangles), where the dye cation and dye excitons absorb, without (upper panel) and with Li-TFSI (lower panel) along with the fits (solid lines) according to the model explained in the text.

In sample 1 the decay kinetics in these three wavelength regions are all due to the decay of dye excitons to the ground state. As already observed in the spectra the signals decayed to zero within the measured time range, indicating that no long lived charges were created. However, the kinetics of the wavelength regions identified are slightly different. We have measured the transient absorption decay of this dye in solution with a sequence of solvents of differing polarity (see Supporting Information). The decay time of the exciton and its absorption spectra was affected by the solvent polarity, indicating that the dielectric environment has an influence on the photoinduced spectrum of the dye exciton and its relaxation kinetics. This is not surprising, as the dye exhibits a strong donor-acceptor character and thus has high electric dipole moments. Based on this knowledge we interpret the transient absorption data of sample 1 in the following way. Due to the distribution of surface binding angles (i.e., how much the dye stands or lies on the surface) and the disorder of the titania surface[26] there are a variety of effective local dielectric environments that the dye excitons experience in sample 1. This inhomogeneously broadened distribution of dye excitons causes the measured decay to be non-exponential and also vary with wavelength.

Due to this inhomogeneous broadening, it is difficult to reconstruct exactly the population kinetics of exciton decay in

sample 1 (at least without explicit knowledge of the distribution of cross-sections which is difficult to obtain).

However, without an explicit knowledge of the population kinetics in sample 1 we can still get an estimate for *f*. We can parameterize the signal from sample 1 somehow, let us call this parameterization $\Delta T/T_{s1}^{P}$, in order to express how a randomly distributed exciton population decays. We can then express the decay of sample 2 as shown in Equation (1), where we assume that a fraction of the initial population *f* injects charges (due to the influence of Li-TFSI as already established) leading to a transient absorption signal $\Delta T/T_{\text{charges}}$, while the remaining $(1-f)$ part of the population leads to the exciton decay signal that we have already parameterized.

$$\Delta T/T_{s2} = f\,\Delta T/T_{\text{charges}} + (1-f)\,\Delta T/T_{s1}^{P}. \quad (1)$$

To parameterize the signal observed in sample 1 we fit the kinetic at each wavelength range to the sum of three exponentials ($\sum_{i=1}^{3} A_i^{\lambda}\exp(-k_i t)$). As shown in Figure 6 this provides an accurate representation of the signal.

We now must come up with a model for the contribution of the charge-generating fraction of the population. Due to the presence of the typical dye cation feature from the earliest times, we assume that the dyes that are affected by Li-TFSI inject faster than the response time of our spectrometer (>500 fs). Therefore we initially observe fN_0 dye cations $D^{+}_{+\text{Li}}{}^{(t)}$. As already mentioned, we observe some recombination of dye cations with electrons in the TiO_2 on the timescale of our experiment; this is seen in a decrease of the blue line between 100 and 1000 ps in Figure 6b. However, after longer times (1000 ps and longer), the signal levels off and the dye cations recombine on a much longer timescale (see Supporting Information). To account for this, we split the dye cations in two pools: one is prone to fast recombination (fraction *s*) with the rate $k_{\text{D}+\rightarrow\text{D}}$ and the other (fraction $1-s$) does not recombine on the observed timescale. Considering the inhomogeneous broadening observed in the exciton population, we feel that this approximation of different lifetime scales for recombination is reasonable. Under these assumptions the transient absorption of the charges can be written as:

$$\Delta T/T_{\text{charges},\lambda} = N_0 d f \sigma_{\lambda,\text{D}+}\left[s\,\exp(-k_{\text{D}+\rightarrow\text{D}}t) + (1-s)\right. \quad (2)$$

Substituting Equation (2) into Equation (1) we can fit the transient absorption kinetics recorded for sample 2 with the free parameters *f*, *s*, $k_{\text{D}+\rightarrow\text{D}}$, and also a dye cation cross-section $\sigma_{\lambda,\text{D}+}$ for each wavelength region. $N_0 d$ is the number of absorbed photons per area (excitation density times thickness of the sample), determined by the pump fluence and the absorbance of the sample at the excitation wavelength. The result of the fit is shown in Figure 6b and the extracted parameters are summarized in **Table 1**. The modeling of the transient absorption of sample 1 and sample 2 reveals a fraction f = 68% of dye excitons that undergo type I charge generation. This means that 32% of dye excitons cannot generate charges by a type I mechanism in this dye system. We also found that roughly 60% of the charges created by the type I mechanism in sample 2 are susceptible to fast recombination, but we will see that when the hole transporter is added in sample 3 this quick recombination is suppressed so it does not affect device efficiency.

Table 1. Parameters obtained from analysis of the transient absorption of sample 1 and 2 described in the text.

Parameter	805 nm	900 nm	1500 nm
$N_0 d$/ (10^{13}cm^{-2})	3.16 ± .33		2.95 ± .46
$k^{-1}_{\text{D}^+\rightarrow\text{D}/\text{ps}}$	1011 ± 117		
f	0.68 ± .02		
s	0.62 ± .02		
$\sigma_{\text{D}^+/(10^{-17}\text{cm}^2)}$	3.49 ± .06	6.87 ± .11	1.57 ± 0.04

The error of $N_0 d$ was determined by Gaussian error propagation from the error prone results of fluence and absorbance. All other errors were determined from the fitting.

2.2.7. Transient Kinetics: Sample 3 (Quantum Efficiency Enhancement due to Type II Charge Generation)

The device-like sample 3 now includes the hole transport material. This means that the dye cations created by ultrafast type I charge generation can now be reduced by transferring their holes to the hole transport material. Also it raises the possibility that the $(1-f)$ remaining excitons are quenched by type II charge generation. The transient absorption kinetics of sample 3 are shown in **Figure 7**. The 1400–1600 nm kinetics show a very clear increase on the timescale from 2–20 ps indicating an increase in the population of holes on the hole transport material. This is strongly correlated with a decrease in the dye exciton photoinduced absorption (800–810 nm signal). This correlated increase of the spiro cation absorption and decrease of the exciton photoinduced absorption, plus the fact that the dye cation regeneration has already taken place on the sub 2 ps timescale (see Supporting Information) indicates that type II charge generation occurs in the population of $(1-f)$ excitons that do not undergo type I charge generation.

In order to quantify the role of type II charge generation in the overall efficiency of charge generation we develop a simple population model to describe the population flows after 2 ps in sample 3. This model is summarized in Figure 7a. First, we assume that we can express the excitons with a single spectrum and decay rate to the ground state. Although we know this is only approximately valid from the transient absorption data for sample 1, it is sufficient to obtain the rough estimate of the effect of type II charge generation that we wish. We then assume that the $(1-f)$ excitons that do not undergo type I charge generation can be separated into two pools, those that can undergo type II charge generation (χ_{II}), and those $1-\chi_{II}$ that cannot (perhaps having an unfavorable orientation relative to the hole transport material for hole transfer). The component of excitons that cannot undergo type II generation is necessary to fit the decay in the visible spectra on the timescale of roughly 100 ps. The rate of hole transfer from the exciton to the hole transport material eventually creating free charges is given

DOI: 10.1002/aenm.201300640

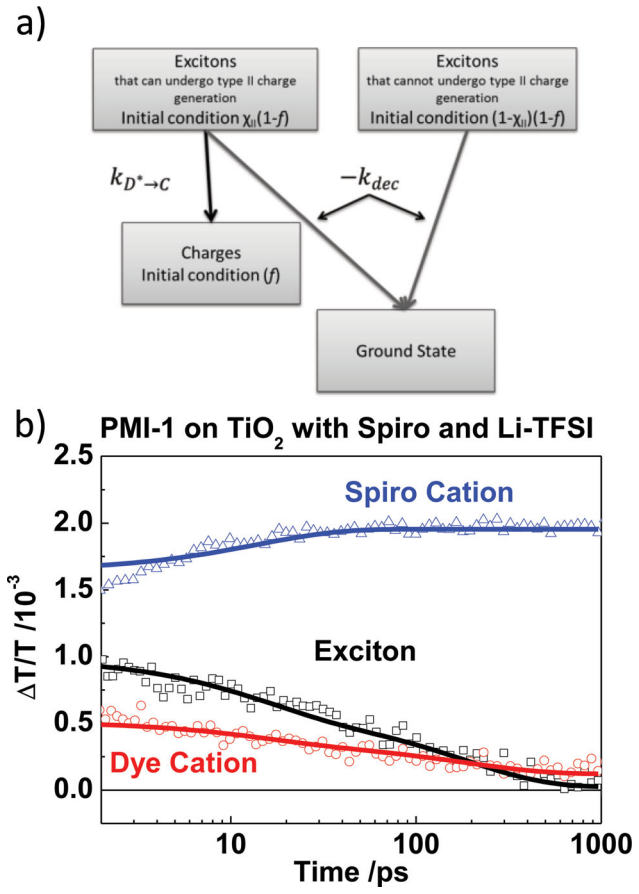

Figure 7. a) Model used to describe the data. b) Transient absorption kinetics of a solar cell probed in three distinct wavelength regions around 805 nm, 900 nm and 1500 nm, where the dye excitons, cations and the cation of the hole transporter dominate the photoinduced absorption, respectively. Along with the experimental data a fit to the model in (a) and as described in the text is shown that was used to determine the possibility of preceding hole transfer (type II charge generation).

by $k_{D^*\rightarrow C}$, and the rate of exciton decay by k_{dec}. The transient absorption kinetics can then be simulated by:

$$\frac{\Delta T}{T}(t,\lambda) = N_0 d\left\{\sigma_{\lambda,D^*}(1-f)\exp(-k_{dec}t)\left[(1-\chi_{II})+\chi_{II}\exp(-k_{D^*\rightarrow C}t)\right] + \sigma_{\lambda,C}\left[f+\frac{\chi_{II}(1-f)k_{D^*\rightarrow C}}{k_{dec}+k_{D^*\rightarrow C}}(1-\exp(-(k_{dec}+k_{D^*\rightarrow C})t))\right]\right\} \quad (3)$$

Where σ_{λ,D^*} and $\sigma_{\lambda,C}$ are the cross-sections of the excitons and the charges (hole on hole transporter) in the wavelength region λ. f was fixed to 0.68, the value from the previous section. The free parameters were k_{dec}, $k_{D^*\rightarrow C}$ and χ_{II}, shared between all wavelength regions, and σ_{λ,D^*} and $\sigma_{\lambda,C}$, which were free for each wavelength region.

The fit is shown in Figure 7b and it is clear that the model can qualitatively describe the features of the data adequately. The parameters extracted from the fits are shown in **Table 2**. The observation of the infrared transient absorption, where the induced absorption of the spiro cation plays a dominant role (see Supporting Information), was critical in revealing the dynamics of type II charge generation, and highlights the utility of broadband spectroscopy for directly revealing population kinetics.

Table 2. Parameters obtained from fitting the transient absorption dynamics of the device-like sample 3 according to the model described in the text.

Parameter	805 nm	900 nm	1500 nm
$N_0 d$ / (10^{13}cm^{-2})	1.78 ± .20		1.88 ± .26
k_{dec}^{-1}/ps	187 ± 20		
$k_{D^*\rightarrow C}^{-1}$/ps	15 ± 3		
χ_{II}	0.44 ± .03		
σ_{λ,D^*}/ (10^{-17}cm^2)	17.2 ± .55	7.34 ± .36	$0^{.89}_{-0}$
$\sigma_{\lambda,C}$/ (10^{-17}cm^2)	0.16 ± .06	0.83 ± 0.06	12.8 ± 0.25
η	81 ± 1%		

The quantum efficiency of charge generation can be calculated as the fraction of excitons which generate charges as $\eta = f + \frac{\chi_{II}(1-f)k_{D^*\rightarrow C}}{k_{dec}+k_{D^*\rightarrow C}}$, where the second half of the expression gives the increase in efficiency due to the type II charge generation. Using the parameters obtained from the fit $\eta = 0.81$, with type II charge generation responsible for around 13% of the total charge generation. We note that this fit can also be performed with f as a free parameter (shared between the wavelengths). This fit is shown in the Supporting Information, and the extracted value for f is 0.53, $\eta = 0.71$, with then type II charge generation making a 20% contribution to the overall charge generation efficiency. Therefore, we conclude that although this modeling is not highly precise, it is certainly sufficient to demonstrate that the overall charge generation efficiency is high, in the region of 0.6–0.9, and that type II charge generation makes a not insignificant contribution, being on the order of 10–30% of the total charge generation.

2.2.8. Kinetics of Spiro:Dye Blend (Verification of Type II Charge Generation)

In the previous section we asserted that type II charge generation (the transfer of a hole from the dye exciton on a surface-bound dye to the hole-transporting spiro) clearly occurred in sample 3, the solar cell structure. If this is the case, then type II charge generation should also occur in a solid-state blend film prepared by spin-casting the dye co-dissolved with the hole-transporting material.[14] In **Figure 8** we present transient absorption data for such a blend film alongside the spectrum of the dye chemically reduced by Lupasol™ treatment. The dye anion absorption peak at around 620 nm is very clear in the transient absorption data, indicating that photoinduced hole transfer indeed causes the creation of a dye anion in this spiro:dye blend.

In order to estimate the rate of type II charge-generation in the blend the data were fit to a two pool (excitons and charge-transfer states) model. The rate of quenching can be seen to be an order of magnitude greater than the dye exciton lifetime in solution, so with the approximation that

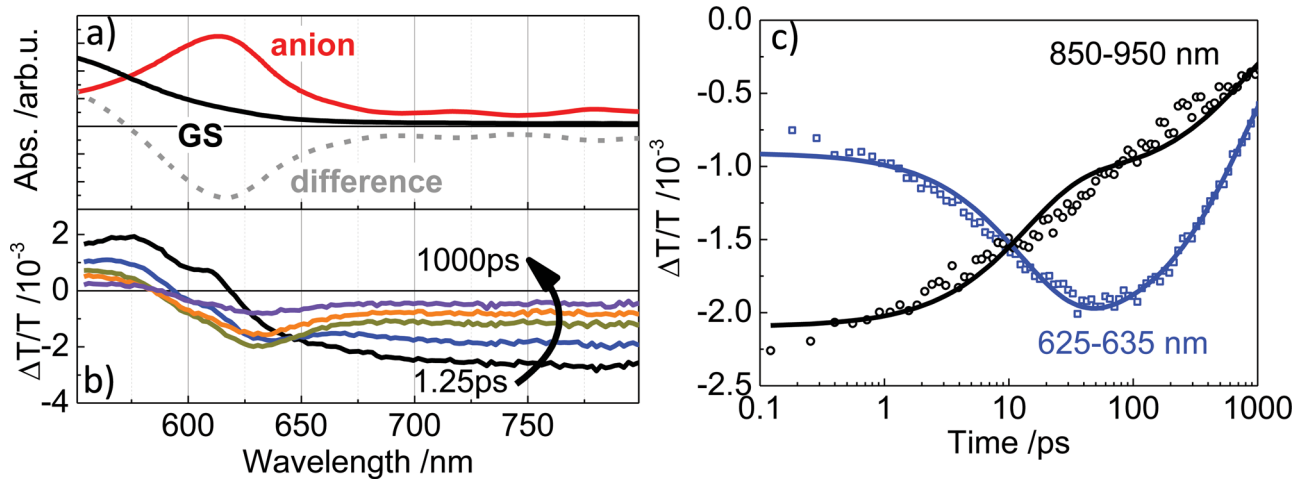

Figure 8. a) Absorption spectra of the ground state (GS, black) and chemically reduced dye (anion, red). The difference spectrum of ground state and anion (dashed grey line) reflects the expected anion-induced absorption signal in the transient absorption spectra. b) Transient absorption spectra of Spiro-MeOTAD:PMI-1 blend; colors refer to times as: black: 1.25 ps; blue: 11 ps; green: 103 ps; orange: 310 ps; purple: 934 ps. Note that after 11 ps the spectrum is very similar to the difference spectrum of ground state and cation-induced absorption (dashed grey line) in the upper panel. c) Transient absorption dynamics for two distinct wavelength regions, in which the absorption of the anion is very prominent (625–635 nm) and in which the exciton absorption dominates the spectrum (900–1000 nm) along with fits to the charge transfer and recombination model explained in the text. The extracted inverse rate for the charge transfer from dye excited state to spiro was (14 ± 1) ps and the inverse recombination rate turned out to be (787 ± 22) ps.

$k_{Ex\rightarrow CT} \gg k_{Ex\rightarrow GS}$ the exciton population can be written as $Ex(t) = \exp(-(k_{Ex\rightarrow CT})t)$ and the charge-transfer state population as $CT(t) = \frac{k_{Ex\rightarrow CT}(\exp(-k_{CT\rightarrow GS}t)-\exp(-k_{Ex\rightarrow GS}t))}{k_{Ex\rightarrow CT}-k_{CT\rightarrow GS}}$.

Here, $k_{Ex\rightarrow CT}$ is the rate of hole transfer from the excited dye to the hole transporter spiro-MeOTAD, $k_{CT\rightarrow GS}$ is the recombination rate of the charge transfer state formed between the dye anion and the spiro cation. Applying this population model to the TA data results in the fits shown as the solid lines. The inverse rates were extracted to be $k^{-1}_{Ex\rightarrow CT} = (14 \pm 1)$ ps and $k^{-1}_{CT\rightarrow GS} = (787 \pm 22)$ ps. Complete details of the fit and the extracted cross-sections are reported in the Supporting Information. The inverse rate of type II charge generation we extracted from sample 3 was (15 ± 3) ps, which agrees well with the rate extracted in the blend film. So examining the blend film gives unequivocal evidence of the formation of dye anions by type II charge generation, and supports our assertion that type II charge generation also occurs in sample 3 given the rate constants agree so well. We note that we do not see the anion feature in sample 3 because anions created at the interface are quickly oxidized by electron injection into the TiO_2 (and overlap with the Stark feature obscures any subtle presence).

Conclusions

We have investigated the use of a perylene monoimide dye in a solid-state dye-sensitized solar cell using steady-state, quasi-steady-state, and time-resolved spectroscopy.

Quasi-steady-state spectroscopy revealed that the presence of Li^+ at the interface was necessary for type I charge generation (electron injection from the excited dye into TiO_2 and subsequent regeneration by the hole transporter), and further time-resolved measurements quantified that around 50–70% of dye excitons can undergo type I charge injection. Steady-state spectroscopy revealed that Li^+ indeed does localize to an extent at the interface, and that the effect of this surface adsorbed Li^+ is to create a field that encourages electron injection into the titania.

Next, our broadband transient measurements allowed us to ascertain that type II charge generation (transfer of the hole from a dye exciton to the hole transport material followed by electron injection from the resulting dye anion into the titania, also known as reductive quenching) also occurs in the solar cell and is responsible for 10–30% of the total charge generation. The general result of this observation is as follows. In the design of low bandgap red-absorbing dyes the LUMO offset from the TiO_2 is often reduced, leading to marginal type I charge injection and a potential loss in quantum efficiency. In order to circumvent this quantum efficiency loss type II charge generation (hole transfer preceding electron transfer) can be targeted. Our results suggest that in order to design a system reaching maximum performance through type II charge generation a lowest unoccupied molecular orbital (LUMO) comparable to the conduction band of TiO_2 should be targeted and then the highest occupied molecular orbital (HOMO) offsets between the dye and the hole transporter material maximized (within the constraint of the dyes HOMO-LUMO offset). Also, finding a structure that is compatible with good electronic overlap between the dye and the hole transport material is important. We find that the perylene monoimide dye investigated is a good model compound for such a system, and can undergo type II charge generation with an inverse rate of (15±3) ps. Type I generation is still marginal in this system, and it may be ideally beneficial to decrease the LUMO of this system somewhat more in order to further increase red absorption (while maintaining the quantum efficiency through an increase in the reliance on the type II mechanism for charge generation). It would of course also be beneficial to increase the rate of type II generation, and

DOI: 10.1002/aenm.201300640

here dye structures that promote intimate contact with the hole transporter material would be interesting.

Supporting Information

Supporting Information is available from the Wiley Online Library or from the author.

Acknowledgment

I.A.H. and M.M. contributed equally to this work. F.L. is very grateful to the Max Planck Society for funding a Max Planck Research Group. M.M. thanks the Max Planck Graduate Center with the University of Mainz (MPGC) for funding. I.A.H acknowledges a fellowship of the Alexander von Humboldt Foundation and a research scholarship of the Max Planck Society. The authors acknowledge financial support from the International Research Training Group 1404 and the SFB 625. F.L. and M.M. thank A. Petrozza for fruitful discussions.

Received: June 8, 2013
Published online:

[1] B. O'regan, M. Gratzel, *Nature* **1991**, *353*, 737.
[2] A. Yella, H.-W. Lee, H. N. Tsao, C. Yi, A. K. Chandiran, M. K. Nazeeruddin, E.W.-G. Diau, C.-Y. Yeh, S. M. Zakeeruddin, M. Grätzel, *Science* **2011**, *334*, 629.
[3] I. Chung, B. Lee, J. He, R. P. H. Chang, M. G. Kanatzidis, *Nature* **2012**, *485*, 486.
[4] J. A. Chang, J. H. Rhee, S. H. Im, Y. H. Lee, H.-j. Kim, S. I. Seok, M. K. Nazeeruddin, M. Gratzel, *Nano Lett.* **2010**, *10*, 2609.
[5] J. Burschka, A. Dualeh, F. Kessler, E. Baranoff, N.-L. Cevey-Ha, C. Yi, M. K. Nazeeruddin, M. Grätzel, *J. Am. Chem. Soc.* **2011**, *133*, 18042.
[6] U. Bach, D. Lupo, P. Comte, J. E. Moser, F. Weissortel, J. Salbeck, H. Spreitzer, M. Gratzel, *Nature* **1998**, *395*, 583.
[7] L. Schmidt-Mende, S. M. Zakeeruddin, M. Gratzel, *Appl. Phys. Lett.* **2005**, *86*, 013504.
[8] C. Li, H. Wonneberger, *Adv. Mater.* **2012**, *24*, 613.
[9] V. Kamm, G. Battagliarin, I. A. Howard, W. Pisula, A. Mavrinskiy, C. Li, K. Mullen, F. Laquai, *Adv Energy Mater* **2011**, *1*, 297.
[10] C. Huang, S. Barlow, S. R. Marder, *J. Org. Chem.* **2011**, *76*, 2386.
[11] U. B. Cappel, M. H. Karlsson, N. G. Pschirer, F. Eickemeyer, J. Schöneboom, P. Erk, G. Boschloo, A. Hagfeldt, *J. Phys. Chem. C* **2009**, *113*, 14595.
[12] U. Bach, Y. Tachibana, J.-E. Moser, S. A. Haque, J. R. Durrant, M. Gratzel, D. R. Klug, *J. Am. Chem. Soc.* **1999**, *121*, 7445.
[13] H. J. Snaith, A. Petrozza, S. Ito, H. Miura, M. Grätzel, *Adv. Funct. Mater.* **2009**, *19*, 1810.
[14] U. B. Cappel, A. L. Smeigh, S. Plogmaker, E. M. J. Johansson, H. k. Rensmo, L. Hammarstrom, A. Hagfeldt, G. Boschloo, *J. Phys. Chem. C* **2011**, *115*, 4345.
[15] H.-S. Kim, C.-R. Lee, J.-H. Im, K.-B. Lee, T. Moehl, A. Marchioro, S.-J. Moon, R. Humphry-Baker, J.-H. Yum, J. E. Moser, M. Gratzel, N.-G. Park, *Sci. Rep.* **2012**, *2*, 591.
[16] M. M. Lee, J. Teuscher, T. Miyasaka, T. N. Murakami, H. J. Snaith, *Science* **2012**, *338*, 643.
[17] A. Hagfeldt, G. Boschloo, L. Sun, L. Kloo, H. Pettersson, *Chem. Rev.* **2010**, *110*, 6595.
[18] H. J. Snaith, M. Gratzel, *Appl. Phys. Lett.* **2006**, *89*, 262114.
[19] G. Boschloo, A. Hagfeldt, *Inorg. Chim. Acta* **2008**, *361*, 729.
[20] M. D. Brown, T. Suteewong, R. S. S. Kumar, V. D'Innocenzo, A. Petrozza, M. Lee, U. Wiesner, H. J. Snaith, *Nano Lett.* **2010**, *11*, 438.
[21] C. Olson, D. Veldman, K. Bakker, F. Lenzmann, *Int. J. Photoenergy* **2011**, *2011*, 513089.
[22] U. B. Cappel, E. A. Gibson, A. Hagfeldt, G. Boschloo, *J. Phys. Chem. C* **2009**, *113*, 6275.
[23] U. B. Cappel, S. M. Feldt, J. Schöneboom, A. Hagfeldt, G. Boschloo, *J. Am. Chem. Soc.* **2010**, *132*, 9096.
[24] S. Ardo, Y. Sun, A. Staniszewski, F. N. Castellano, G. J. Meyer, *J. Am. Chem. Soc.* **2010**, *132*, 6696.
[25] M. Meister, B. Baumeier, N. Pschirer, R. Sens, I. Bruder, F. Laquai, D. Andrienko, I. A. Howard, *J. Phys. Chem. C* **2013**, *117*, 9171.
[26] S. Ardo, G. J. Meyer, *Chem. Soc. Rev.* **2009**, *38*, 115.